American Mineralogist, Volume 81, pages 719–734, 1996

Experimental partitioning of Rb, Cs, Sr, and Ba between alkali feldspar and peraluminous melt

JONATHAN ICENHOWER AND DAVID LONDON

School of Geology and Geophysics, University of Oklahoma, 100 East Boyd Street, SEC 810, Norman, Oklahoma 73019, U.S.A.

ABSTRACT

Hydrous partial melting experiments performed between 650 and 750 °C at 200 MPa (H_2O) on synthetic metapelite compositions (quartz + albite + muscovite + biotite mineral mixtures) doped with Ba, Sr, Rb, and Cs yielded alkali feldspar crystals with a wide range of compositions in equilibrium at their rims with peraluminous melt. Measured partition coefficients for normally trace lithophile elements between feldspar and melt [$D(M)^{Fsp/gl}$, M = Ba, Sr, Rb, Cs] do not depend on either temperature or bulk composition of melt for the compositions studied. Values of $D(Sr)^{Fsp/gl}$ are between 10 and 14 and appear to be independent of the albite and orthoclase contents of the feldspar crystals. In contrast, values of $D(Ba)^{Fsp/gl}$ and $D(Rb)^{Fsp/gl}$ are strongly dependent on the orthoclase content of feldspar, relationships that can be expressed by the following linear equations: $D(Ba)^{Fsp/gl} = 0.07 + 0.25(\text{orthoclase})$ and $D(Rb)^{Fsp/gl} = 0.03 + 0.01(\text{orthoclase})$, where orthoclase is in mole percent. These equations reproduce the range of previously reported values for $D(Ba)$ and $D(Rb)$ determined on natural and synthetic samples. A single partition coefficient for Cs was also determined at $D(Cs)^{Fsp/gl} = 0.13$.

These data can be used in conjunction with recently published partition coefficients for muscovite, biotite, and plagioclase feldspars (Blundy and Wood 1991; Icenhower and London 1995) to model quantitatively the trace element signatures of peraluminous magmas during anatexis and crystallization. Depending on bulk composition and pressure-temperature trajectories during episodes of partial melting, Ba and Sr (and to a lesser extent, Rb) are retained at the source while Cs and Li are enriched in the first melts. These results explain why peraluminous granitic magmas with S-type (sedimentary) sources carry a distinctive enrichment in Li and Cs.

INTRODUCTION

Partition coefficients for the large-ion lithophile elements (LILEs) Ba, Sr, Rb, and Cs between alkali feldspar and intermediate to silicic melt have been investigated by Arth (1976), Berlin and Henderson (1969), Carmichael and McDonald (1961), Carron and Lagache (1980), De Pieri and Quareni (1978), Ewart and Taylor (1969), Guo and Green (1989), Higuchi and Nagasawa (1969), Leeman and Phelps (1981), Long (1978), Mahood and Hildreth (1983), Nagasawa and Schnetzler (1971), and Nash and Crecraft (1985), to name a few. Despite the volume of previous work little consensus has emerged regarding the true values of these partition coefficients. Differences in comparable studies may be as much as an order of magnitude; therefore, selection of any particular value for petrogenetic modeling becomes a difficult if not arbitrary choice. It is not surprising therefore, that some investigators have suggested that distribution coefficients determined on one suite of rocks cannot be used to model the evolution of another (cf. Mahood and Hildreth 1983).

Variation in melt composition, or melt structure, has been advanced as one key component in governing distributions of trace elements between crystals and melt (Watson 1976, 1977; Ryerson and Hess 1978; Hart and Davis 1978; Mysen and Virgo 1980; Carron and Lagache 1980). The experimental study by Watson (1976) laid the groundwork for models of element distribution as a function of melt structure, measured as the ratio of inferred network-modifying to network-forming (tetrahedrally coordinated) species in melt. The two-liquid study by Watson (1976) assessed the preference of a trace element to partition into Si-rich or Si-poor melt. Generally, trace elements partitioned increasingly into the less siliceous melt as the cation field strength (Z/r^2) increased. Among the LILEs, the cations with the highest field strengths (e.g., Ba) tended to favor Si-poor melt, whereas Cs was the only LILE to partition in favor of the more siliceous melt. The general trends identified by Watson (1976) are consistent with variations in enthalpies of mixing along $M^{n+}_{1/n}AlO_2$-SiO_2 joins, where M = alkali and alkaline earth cations (Roy and Navrotsky 1984). Carron and Lagache (1980) proposed that partitioning of Rb, Cs, Sr, and Ba between alkali feldspar and melt is strongly influenced by the Na/K ratio of melt; however, partition coefficients for LILEs between alkali feldspar and melt were not directly determined.

The composition and hence the structure of the crys-

0003–004X/96/0506–0719$05.00

talline phase also strongly influence partition coefficients (Matsui et al. 1977; Blundy and Wood 1991). In particular, the study by Blundy and Wood (1991) demonstrated that partitioning of Sr and Ba between plagioclase and melt depends on the anorthite content of feldspar; albitic feldspars accept both Sr and Ba more readily than anorthitic. It is not clear, though, how the orthoclase content in alkali (or ternary) feldspars affects partitioning of these elements and Rb and Cs. The study of Smith and Brown (1988) showed that, in general, partition coefficients for Rb and Ba increase with orthoclase content of feldspar. The scatter of data, however, prevents a quantitative assessment of this effect on partitioning.

Other parameters that may influence partitioning behavior include temperature (Drake 1972; Sun et al. 1974; Nielsen 1988; Guo and Green 1989) and pressure (Green and Pearson 1983; Guo and Green 1989). Blundy and Wood (1991) argued that a relationship between temperature and partition coefficients for Sr and Ba in plagioclase-series feldspars is simply an artifact of feldspar compositional changes (i.e., albitic plagioclase is stable at lower temperatures than anorthitic plagioclase). Although pressure appears to be an important factor governing trace element partitioning, the experiments of Guo and Green (1989) may not be relevant to peraluminous igneous systems. As discussed below, their experiments were performed on peralkaline compositions at higher pressures than the pressures at which feldspar and melt typically coexist in peraluminous systems (Thompson and Tracy 1979).

The above studies serve as an important guide for investigating the partitioning behavior of the LILEs. In this investigation we report experimentally determined partition coefficients for Rb, Cs, Ba, and Sr between alkali feldspars and peraluminous melt generated by water-saturated partial melting and recrystallization of synthetic metapelite compositions. We chose our bulk compositions to replicate peraluminous two-mica granites and rhyolites that are exposed as volumetrically important constituents of the Himalayas, the Hercynian massifs, and numerous igneous bodies in the American southwest (Le Fort et al. 1987; Wickham 1987; Anderson 1983). The relatively simple mineralogy of these leucogranites affords the opportunity to model their LILE signatures using established trace element partitioning equations. These elements are especially useful for determining conditions of melting and crystallization because the LILEs are principally harbored by major crystalline phases (feldspars, biotite, muscovite) and do not reside in accessory minerals (e.g., zircon, monazite, apatite, xenotime) the solubilities of which are highly variable in these melts (Hogan and Sinha 1991; Montel 1986; Watson and Harrison 1983; Wolf and London 1994).

The experiments were conducted at low pressures (200 MPa) in part to replicate magma crystallization at higher levels in the crust, and at H_2O saturation to represent possible end-member scenarios at the most hydrous stages of melt evolution; i.e., at the inception of anatexis and at the close of crystal fractionation. All experiments were saturated in corundum, fixing the activity of Al_2O_3 in melt at unity. Therefore, the K/Na ratio of melt can vary without changing the activities of most melt components. The data presented here on alkali feldspars, along with complementary studies of biotite, muscovite, cordierite, and garnet (e.g., Icenhower and London 1993a, 1993b, 1995; Icenhower et al. 1994) are therefore intended to constrain the chemical signatures of peraluminous melts to assist others in identifying fractionation trends within and source regions of S-type granites and related rocks.

Methods

Compositions corresponding to synthetic metapelites were made up of mixtures of natural muscovite, albite, quartz, and biotite. Muscovite was separated from a recrystallized muscovite-tourmaline schist near a contact with the Strickland-Cramer pegmatite body, Portland, Connecticut (DL sample STK-127); microprobe analyses presented in Table 1 indicate that it is characterized by relatively high concentrations of F (~1.3 wt%) and low TiO_2 (0.44%), MgO (0.76%), FeO (2.73%) (all iron as FeO), and Na_2O (0.39%). In addition, the muscovite contains ~2275 ppm Li (or ~0.4 wt% Li_2O) as determined by inductively coupled plasma (ICP) spectroscopy. Microprobe analyses of the starting plagioclase (Table 1) from Minas Gerais, Brazil, reveal that it is near end-member albite. The quartz used was high-purity electronic grade, with <50 ppm total impurities (kindly provided by Feldspar Corporation, Spruce Pine, North Carolina). Concentrations of SrO, BaO, Rb_2O, and Cs_2O in all three minerals, as determined by microprobe analysis, are below their respective detection limits. The starting biotite is a Li-, Cs-, Rb-, and F-rich metasomatic mica from the amphibolitic wall rocks of the Tanco pegmatite, Manitoba (Table 1; Morgan and London 1987). In addition, this mica contains ~2.15 wt% Li_2O. We used this mica as a source of Li, Rb, Cs, and F. At the conditions of our experiments, it reacts (dissolves) almost completely and reprecipitates as a new mica in equilibrium with melt. Thus, there is no problem in distinguishing relict mica grains from those that have recrystallized and chemically equilibrated with (precipitated from) the melt.

The minerals were mixed in such a way that biotite made up 30 wt% of the total mix. The amounts of muscovite, albite, and quartz were varied to impart a range of K/Na ratios to the starting compositions. Starting compositions, labeled "Synpel" for synthetic metapelite, are tabulated in Table 2. Note that in all three of the starting mineral mixes, quartz is the limiting component of melting because we wanted muscovite to survive in the presence of melt (see below).

The starting compositions were designed to have concentrations of normally trace elements that are measurable with high accuracy by electron microprobe analyses (EMPA). Lithophile elements Sr and Ba were added to

TABLE 1. Compositions of starting minerals

	Albite $n = 40$	Muscovite $n = 37$	Biotite $n = 84$	Andalusite $n = 30$	Cordierite $n = 25$
		Weight percent			
SiO_2	68.22(0.25)	45.92(0.28)	40.12(0.84)	36.15(0.16)	48.39(0.25)
TiO_2		0.44(0.15)	1.19(0.14)		*0.04*
Al_2O_3	19.95(0.19)	33.83(0.63)	17.56(0.38)	63.65(0.26)	33.72(0.13)
MgO	*0.02*	0.76(0.07)	7.25(0.24)		12.56(0.10)
CaO	0.03(0.03)	*0.02*	*0.02*		*0.02*
MnO		0.21(0.03)	0.23(0.03)	*0.04*	0.06(0.02)
Li_2O*		0.46	2.17		
FeO	*0.02*	2.73(0.14)	8.13(0.61)	0.31(0.02)	2.55(0.07)
Fe_2O_3**			2.26		
NiO		*0.04*	*0.04*		
SrO	*0.07*	0.09(0.09)	0.14(0.15)		
BaO	*0.13*	*0.13*	*0.13*		
Na_2O	11.45(0.13)	0.39(0.04)	*0.02*		0.30(0.02)
K_2O	0.21(0.03)	10.69(0.10)	6.78(0.33)		*0.02*
Rb_2O	*0.05*	*0.05*	3.82(0.07)		*0.05*
Cs_2O	*0.11*	*0.11*	3.83(0.59)		*0.11*
H_2O†		3.78(0.08)	1.42(0.13)		
F		1.30(0.12)	4.58(0.29)		*0.17*
P_2O_5	0.03(0.02)				
Total	100.29	100.91	99.69	100.15	97.97
O = F		100.36	97.76		
		Cations pfu			
Normalization basis	8(O)	24 (O, F, OH)	24 (O, F, OH)	20 (O)	18 (O)
Si	2.98	6.16	6.16	3.91	4.90
$^{[4]}Al$		1.84	1.84		
Ti		0.04	0.14		0.00
$^{[6]}Al$	1.03	3.51	1.34	8.11	4.03
Mg	0.00	0.15	1.66		1.90
Mn		0.02	0.03	0.00	0.00
Li		0.25	1.34		
Fe^{2+}	0.00	0.31	1.04	0.03	0.22
Fe^{3+}			0.26		
Ni		0.00	0.00		
Ca	0.01	0.00	0.00		0.00
Sr	0.00	0.01	0.01		
Ba	0.00	0.00	0.00		
Na	0.95	0.10	0.00		0.06
K	0.02	1.83	1.33		0.00
Rb	0.00	0.00	0.38		0.00
Cs	0.00	0.01	0.25		0.00
Total	4.98	14.23	15.78	12.05	11.10
Ab	0.97	Mg′ = 0.32‡	Mg′ = 0.61		Mg′ = 0.90
Or	0.02				
An	0.01				

Note: Numbers in parentheses represent standard errors. Numbers in italics represent detection limits. Blank = not determined.
* Li_2O determined by ICP.
** Fe_2O_3 determined by titration.
† H_2O estimated by stoichiometry.
‡ Mg′ = molar Mg/(Mg + Fe + Mn).

the mineral mixes as glasses of celsian ($BaAl_2Si_2O_8$) and slawsonite ($SrAl_2Si_2O_8$). The concentrations of LILEs in the starting mineral mixes were 2 wt% each SrO and BaO and 1.15 wt% each Rb_2O and Cs_2O (from starting biotite; Table 2). The apparent high concentrations of these oxide components were diluted by large volumes of melt generated at the peritectic minimum of the system. Therefore, depending on the partitioning behavior of the element, concentrations of the LILEs were brought above but near the lower limits of detection by EMPA for all mineral-melt pairs.

Mixed mineral powders were ground under ethanol in

TABLE 2. Compositions of starting assemblages

	Synpel 5	Synpel 6	Synpel 7
Muscovite	34	27.5	44.3
Quartz	17	13.5	12
Albite	19	29	13.7
Biotite	30	30	30
	Trace element (wt%)		
BaO	2	2	2
SrO	2	2	2
Rb_2O	1.15	1.15	1.15
Cs_2O	1.15	1.15	1.15

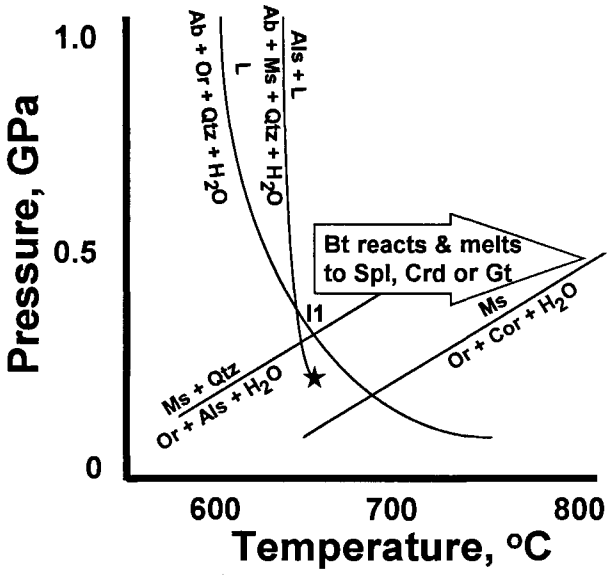

FIGURE 1. Partial P-T phase relations for metapelite-peraluminous granitic systems. Sources of reaction data are (1) muscovite + quartz + albite + H_2O = L + aluminum silicate (Storre and Karotke 1971), (2) muscovite + quartz = orthoclase + aluminum silicate + H_2O (Althaus et al. 1970), (3) muscovite = orthoclase + corundum + H_2O (Yoder and Eugster 1955), and quartz + albite + orthoclase + H_2O = L (Merrill et al. 1970). Invariant point I_1 lies at the intersection of Reaction 2 with the haplogranitic minimum. Reaction 1 is metastable below its intersection with Reaction 2. Along the metastable extension of Reaction 1 to 200 MPa (0.2 GPa), the experimental solidus of the system studied here (between 600 and 650 °C) lies slightly below the star because of the addition of F and other components. Above the solidus of Reaction 1, biotite (Bt) reequilibrates with melt and with increasing T reacts continuously to form melt + spinel (Spl) and cordierite (Crd) or garnet (Gt).

an agate mortar and then dried overnight in an oven at 150 °C. Gold capsules measuring 1 cm × 3 mm × 0.2 mm were loaded with ~20 mg rock powder and ~2 mg distilled water. The capsules were welded, checked for weight loss, then placed in an oven overnight at 150 °C to check for leaks. Successfully sealed capsules were then loaded into cold-seal Rene-41 reaction vessels with stainless steel filler rods and run at 200 MPa. The pressure medium was water plus trace amounts of a hydrocarbon-based rust inhibitor that imposed an f_{O_2} slightly less than the nickel + nickel oxide (NNO) buffer of the reaction vessel. Pressure was monitored by a factory-calibrated Heise Bourdon-tube gauge, and all experiments were conducted in contact with the gauge and with a 2 L pressure buffer; pressure uncertainty is <1 MPa. Temperatures were monitored by internal Chromel-Alumel thermocouples; temperature uncertainty is ±2 °C. Experiments were quenched isobarically in an air jet to <300 °C in 10–50 s. Capsules were weighed after experiments to check for leaks; however, all capsules gained weight (~0.2 mg) because of diffusion of Ni from the reaction vessel into the precious metal capsule. Experimental products were analyzed by optical examination, scanning and back-scattered electron (BSE) imaging, and energy- and wavelength-dispersive X-ray spectroscopy. Quantitative electron microprobe analyses of experimental products were performed using wavelength-dispersive X-ray spectroscopy exclusively. The PAP correction procedure (Pouchou and Pichoir 1984) was applied to the EMPA data; analytical conditions, including beam conditions, diffracting crystals used, counting times, and lower limits of detection (LLDs), are tabulated in the Appendix of Icenhower and London (1995).

CONDITIONS OF MELTING

Partial melting took place along the metastable extension of reaction

$$\text{muscovite} + \text{quartz} + \text{albite} + H_2O = \text{L (melt)} + \text{aluminum silicate} \quad (1)$$

(Storre and Karotke 1971) to 200 MPa, the conditions of our experiments. The reaction is metastable at this pressure because the stable reaction

$$\text{muscovite} + \text{quartz} = \text{orthoclase} + \text{aluminum silicate} + H_2O \quad (2)$$

should proceed to the right. Instead, melting proceeded fast enough that all quartz was consumed before orthoclase could nucleate. The result was that all phases (crystalline and liquid) were stable at these quartz-absent conditions of P and T. The steep negative slope of Reaction 1 is important because it is nearly temperature-independent, allowing us to extrapolate reasonably our observed melting relations to the higher pressures that are more likely for the production of granitic magmas (i.e., 400–600 MPa: Thompson and Tracy 1979). Because our experiments were quartz undersaturated and muscovite oversaturated above the solidus temperature, the next heterogeneous reaction with increasing temperature involved the equilibrium

$$\text{muscovite} = \text{orthoclase} + \text{corundum} + H_2O \quad (3)$$

(Yoder and Eugster 1955) that was encountered near 715 °C at 200 MPa. The importance of this reaction is that very micaceous rocks, such as the Synpel mixtures, contain muscovite above the melting temperature, and both muscovite and biotite contribute K to melt and to the crystallization of alkali feldspar. These reactions also describe partial melting of muscovite-bearing assemblages at pressures greater than the invariant point I_1 of Figure 1. In summary, our experiments yielded alkali feldspars over a temperature range of 100 °C (650–750 °C) and serve as reasonable analogs for partial melting reactions that take place in the crust at higher pressures.

Note that Reactions 1–3 are continuous reactions over a range of P and T because the reactants and products

are solid solutions. The terminal reaction for muscovite (Reaction 3) is quite sharply delineated in P-T space. Reactions involving biotite, however, are continuous from the inception of melting, wherein biotite equilibrates with melt, through continuous melting reactions with increasing T that eventually yield spinel as a distinctive product of biotite breakdown (e.g., Icenhower and London 1995).

Approach to equilibrium

By monitoring the chemical and textural features of experimental products, we established that durations of four weeks were necessary for most experiments to attain textural and chemical steady state. Albite was the sole feldspar in the starting bulk compositions, so the multicomponent potassium sodium calcium feldspar solid solutions we obtained clearly precipitated from melt and do not include unreacted starting material. Feldspars are euhedral in habit but nevertheless display chemical zoning from core to rim (Fig. 2). The zoning indicates that cores are not in equilibrium with final melt compositions, and therefore we carefully limited our analyses only to feldspar rims, which were likely to represent a close approach to equilibrium with melt. We analyzed only homogeneous feldspar rims that were >5 μm thick, and thus we largely ignored the reservoir effects of the feldspar cores. Other evidence that the experiments approached equilibrium (exclusive of feldspar cores) include euhedral and homogeneous biotite and muscovite and uniform distributions of Ba, Rb, Sr, and Cs in melt, as manifested by small standard deviations in glass analyses, suggestive of complete diffusion over the duration of the experiments. Finally, the results of analyses of feldspar, glass, and mica in experiments lasting up to six weeks were not significantly different from the results of experiments lasting four weeks.

We emphasize that experiments of this sort do not lend themselves to true reversals. Reversals would entail equilibration by diffusion of trace elements from melt into crystalline phases and from crystalline phases into melt. In reality, when the mineral-melt compositions are far enough from equilibrium, as they are at the start of melting, the reactions invariably entail the dissolution of minerals and reprecipitation of crystalline phases with compositions that are closer to equilibrium with melt. Put another way, all major and trace elements are redistributed by direct crystallization from melt, which might be regarded as synthesis reactions in that the original crystalline phases rarely constitute nucleation sites for subsequent growth (they are dissolving). In these experiments, we induced reactions from two directions of T: one prograde in T, termed forward direction; and the other retrograde in T, termed reverse direction, but not to be confused with a reversal as described above. The benefits of reverse-direction experiments, as detailed by London (1992) include more complete and rapid homogenization of melt, clear indications of crystal growth, and coarse grain size that facilitates EMPA. Drawbacks include the liquidus undercoolings required to initiate crystallization and the metastable persistence of crystal-melt compositions (i.e., lack of approach to equilibrium) with a large magnitude of undercooling. Forward-direction experiments do not have the same sort of closure T, so our estimation of approach to equilibrium is based on convergence of mineral and melt compositions from forward- and reverse-direction experiments to the same T. In general, these were good in the experiments presented

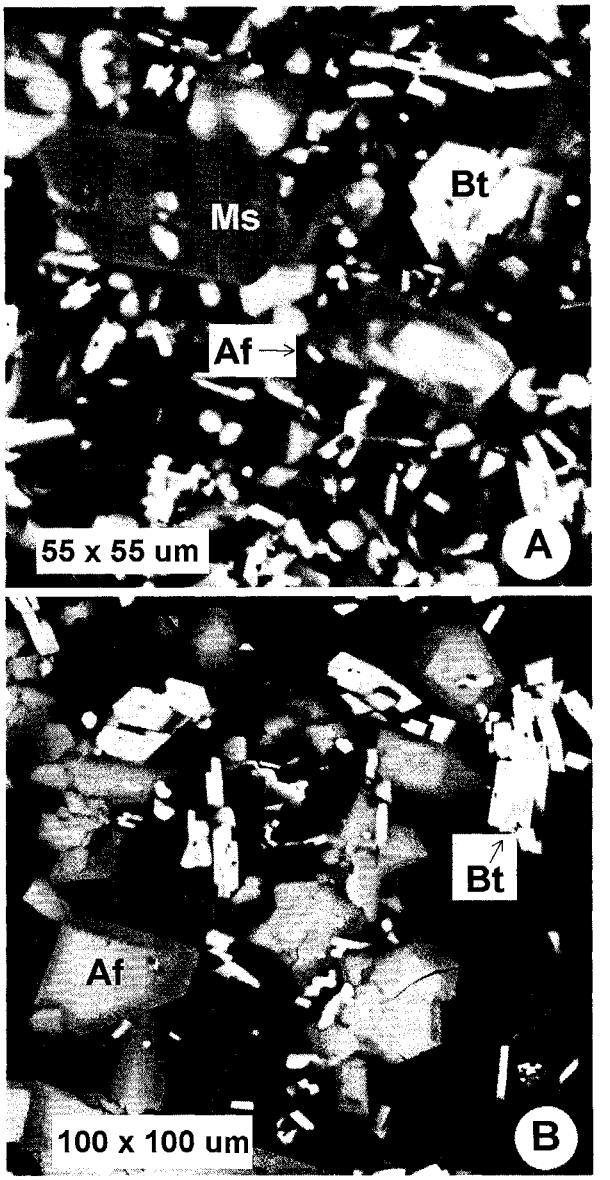

Figure 2. Back-scattered electron images of experimental products. (**A**) Zoned feldspar, biotite, muscovite, and glass in a 650 °C reverse-direction experiment. (**B**) Zoned alkali feldspar, biotite, and glass in a 700 °C forward-direction experiment.

TABLE 3. Glass compositions

Expt.	5 + 15	5 + 14	5 + 8	5 + 7	5 + 5	5 + 9	6 + 6	6 + 5
T (°C)	650, R	650, R	650, R	700, R	700, F	700, F	650, R	700, R
No. analyses	n = 20	n = 10	n = 15	n = 13	n = 18	n = 10	n = 40	n = 22
SiO_2	63.94(0.20)	64.27(0.25)	65.90(0.17)	63.52(0.24)	64.04(0.12)	63.49(0.19)	65.38(0.10)	63.10(0.07)
TiO_2	00.09(0.01)	00.07(0.01)	00.06(0.01)	00.07(0.02)	00.05(0.00)	00.09(0.02)	*00.04*	00.05(0.01)
Al_2O_3	15.84(0.08)	15.67(0.14)	15.61(0.10)	16.93(0.06)	17.00(0.04)	16.58(0.07)	16.24(0.04)	17.27(0.03)
MgO	00.16(0.02)	00.11(0.02)	00.12(0.02)	00.13(0.04)	00.07(0.00)	00.09(0.02)	00.05(0.01)	00.07(0.00)
CaO	00.83(0.01)	00.82(0.01)	00.80(0.02)	00.94(0.01)	01.01(0.01)	00.89(0.02)	00.44(0.01)	00.61(0.01)
MnO	00.07(0.00)	00.07(0.00)	00.08(0.01)	00.06(0.01)	00.07(0.01)	00.08(0.01)	00.05(0.00)	00.06(0.00)
FeO	00.74(0.06)	00.64(0.04)	00.61(0.05)	00.73(0.10)	00.61(0.01)	00.67(0.04)	00.40(0.01)	00.54(0.01)
NiO	*00.04*	*00.04*	*00.04*	*00.04*	*00.04*	*00.04*	*00.04*	*00.04*
SrO	00.45(0.04)	00.21(0.03)	00.22(0.02)	00.43(0.06)	00.40(0.02)	00.41(0.03)	00.11(0.01)	00.32(0.03)
BaO	00.27(0.03)	00.21(0.04)	00.22(0.02)	00.32(0.04)	00.27(0.01)	00.29(0.02)	00.11(0.01)	00.23(0.02)
Na_2O	01.95(0.02)	01.54(0.07)	02.19(0.02)	02.03(0.10)	02.32(0.01)	01.97(0.07)	02.83(0.02)	02.87(0.03)
K_2O	03.28(0.04)	03.13(0.05)	03.29(0.04)	03.77(0.04)	03.86(0.02)	03.46(0.04)	03.25(0.02)	03.45(0.01)
Rb_2O	00.59(0.01)	00.53(0.02)	00.60(0.01)	00.64(0.01)	00.68(0.01)	00.56(0.01)	00.67(0.01)	00.62(0.00)
Cs_2O	01.04(0.02)	01.07(0.03)	01.09(0.03)	00.86(0.02)	00.96(0.01)	00.90(0.03)	01.14(0.01)	00.95(0.01)
F	01.74(0.04)	01.79(0.07)	01.70(0.06)	01.95(0.15)	01.67(0.04)	01.96(0.03)	02.01(0.04)	02.03(0.03)
P_2O_5	00.12(0.01)	00.12(0.01)	00.14(0.01)	00.12(0.01)	00.12(0.00)	00.13(0.01)	00.14(0.00)	00.13(0.00)
Total	91.15	90.29	92.67	92.54	93.17	91.61	92.90	92.34
O = F	90.42	89.54	91.95	91.72	92.47	90.78	92.05	91.46
ASI	01.65	01.86	01.61	01.62	01.53	01.69	01.64	01.61
Mg′	26.02	21.62	23.64	22.66	15.49	17.60	16.51	17.20
K′	41.66	45.08	40.49	44.10	42.13	42.93	37.26	37.62
				CIPW norm				
Q	46.82	52.63	45.94	42.40	39.21	45.19	40.34	36.73
Ab	25.24	20.27	27.19	25.92	29.02	25.43	33.98	35.33
Or	27.94	27.10	26.87	31.68	31.77	29.38	25.68	27.94
Cor	07.43	08.69	06.90	07.55	06.81	07.92	07.25	07.56

Note: F = forward-direction experiment, R = reverse-direction experiment, ASI = molar Al/Σ alkalis + 2Σ alkaline earths, Mg′ = molar 100Mg/(Mg + Fe + Mn), K′ = molar 100K/Σ alkalis + Σ alkaline earths. Numbers in italics represent detection limits.

here (examples provided below), though in some cases a particular element failed to equilibrate (e.g., Sr in reverse-direction experiments).

RESULTS

Phase assemblages in Synpel 5, 6, and 7 contain biotite, muscovite, alkali feldspar, corundum, aluminum silicate, and melt (as glass) in 650 °C reverse- and 700 °C forward-direction experiments, and biotite, alkali feldspar, corundum, and glass ± spinel ± mullite in 750 °C forward- and 700 °C reverse-direction experiments. Melt is present in 650 °C forward-direction experiments but is absent at 600 °C, indicating that the solidus of the system is at an intermediate temperature. Melt makes up at least 50% of the charge by volume at 700 °C with crystals well distributed within the glass. Melt is the dominant phase in forward-direction experiments to 750 °C.

Melt

The compositions of glasses, representing quenched melts, are presented in Table 3. The normative bulk composition at the minimum is approximately $Ab_{30}Or_{15}Ms_{20}Qtz_{35}$, with corundum and orthoclase components combined in equimolar proportions to create a normative muscovite component. Because of the high F contents of the starting micas, all melt compositions contain several normative percent of a cryolite component.

Glasses are silicic (>70 wt% SiO_2 on an anhydrous basis) and extremely aluminous, as denoted by the Al-saturation index, ASI [molar $Al_2O_3/(Na_2O + K_2O + Rb_2O + Cs_2O + CaO + SrO + BaO)$], over the temperature range investigated. Note that the ASI values reported in Table 3 (1.5–1.8) do not factor in Li (derived from melting of both muscovite and biotite in the starting assemblage). From ion microprobe measurements (Icenhower and London 1995), the Li_2O content of glasses is ~0.7 wt%, which when factored in to the expression for ASI lowers the ASI values of glasses to 1.3–1.4. The excess alumina in glass can be recast as a normative corundum component (6.8–8.7 wt%) or as a muscovite component, the anhydrous equimolar sum of normative orthoclase and corundum (approximately 20 wt% muscovite). Concentrations of Al_2O_3 in melt increase with temperature (15.6–16.4 wt% at 650 °C, 18.3–18.5 wt% at 750 °C).

Concentrations of the sum of femic components (TiO_2, MgO, MnO, and FeO) are nearly always <1 wt%, and values of Mg′ [=100Mg/(Mg + Fe + Mn)] are low and vary between 15 and 26, so that the melts correspond to typical leucogranites. The femic sum rises with increasing temperature principally because of a rise in FeO with temperature.

Concentrations of CaO are low (0.4–1.2 wt%) in comparison with Na_2O, which varies between 1.5 and 2.9 wt%, depending on the starting composition. The CaO in these experiments stems from small amounts of plagioclase in the starting biotite separates. K_2O increases with

TABLE 3.—*Continued*

Expt.	6 + 7	6 + 4	7 + 10	7 + 6	7 + 5	7 + 7	7 + 4
T (°C)	700, F	750, F	650, R	650, R	700, R	700, F	750, F
No. analyses	*n* = 38	*n* = 45	*n* = 20	*n* = 20	*n* = 15	*n* = 12	*n* = 20
SiO_2	62.66(0.13)	61.49(0.11)	65.40(0.25)	64.20(0.12)	62.60(0.15)	61.86(0.16)	60.66(0.14)
TiO_2	00.06(0.00)	00.09(0.00)	00.07(0.01)	00.06(0.01)	00.07(0.01)	00.06(0.01)	00.09(0.01)
Al_2O_3	17.42(0.04)	18.34(0.04)	15.88(0.13)	16.37(0.12)	17.09(0.05)	17.28(0.04)	18.48(0.05)
MgO	00.07(0.00)	00.12(0.00)	00.08(0.02)	00.08(0.01)	00.11(0.01)	00.08(0.01)	00.10(0.01)
CaO	00.61(0.01)	00.76(0.01)	00.87(0.01)	00.96(0.01)	01.15(0.01)	00.98(0.01)	01.02(0.01)
MnO	00.06(0.00)	00.07(0.00)	00.06(0.00)	00.07(0.00)	00.08(0.01)	00.08(0.01)	00.09(0.00)
FeO	00.64(0.01)	00.85(0.01)	00.53(0.06)	00.53(0.03)	00.67(0.03)	00.67(0.02)	00.84(0.04)
NiO	*00.04*	*00.04*	*00.04*	*00.04*	*00.04*	*00.04*	*00.04*
SrO	00.19(0.01)	00.50(0.02)	*00.07*	00.20(0.02)	00.24(0.02)	00.39(0.03)	00.65(0.03)
BaO	00.25(0.01)	00.45(0.01)	*00.13*	00.15(0.03)	00.21(0.01)	00.19(0.03)	00.28(0.02)
Na_2O	02.59(0.09)	02.62(0.08)	01.87(0.09)	01.84(0.04)	02.08(0.02)	01.83(0.03)	01.72(0.07)
K_2O	03.43(0.02)	03.61(0.02)	03.95(0.08)	03.50(0.06)	04.21(0.03)	03.79(0.02)	04.90(0.05)
Rb_2O	00.62(0.00)	00.64(0.00)	00.55(0.01)	00.59(0.01)	00.62(0.01)	00.61(0.01)	00.68(0.01)
Cs_2O	00.95(0.00)	00.86(0.01)	01.10(0.02)	01.24(0.02)	01.03(0.02)	01.09(0.02)	00.93(0.02)
F	02.18(0.07)	02.04(0.03)	01.86(0.08)	01.92(0.04)	02.17(0.04)	02.13(0.04)	02.39(0.03)
P_2O_5	00.13(0.00)	00.12(0.00)	00.09(0.01)	00.09(0.01)	00.13(0.01)	00.16(0.01)	00.14(0.00)
Total	91.90	92.60	92.55	91.84	92.50	91.24	93.01
O = F	90.98	91.74	91.77	91.03	91.59	90.34	92.00
ASI	01.72	01.66	01.65	0.170	01.53	01.71	01.60
Mg′	15.12	18.85	19.45	19.18	20.70	15.96	16.07
K′	39.55	39.22	48.36	44.02	45.92	45.65	52.10
				CIPW Norm			
Q	39.23	36.25	44.74	46.54	38.12	42.86	35.38
Ab	32.47	33.44	23.12	23.74	26.54	24.19	22.48
Or	28.30	30.31	32.14	29.72	35.34	32.96	42.14
Cor	08.44	08.39	07.28	07.91	06.84	08.39	07.96

temperature up to the terminal muscovite reaction (~715 °C; cf. Yoder and Eugster 1955) because of the reactions of muscovite and biotite with melt. Above this temperature biotite alone continues to react with melt, liberating K. Values of K′ [=K/(K + Ca + Na + Ba + Sr + Rb + Cs) × 100] vary between ~37 and 52 in the experiments.

Concentrations of BaO and SrO (added as celsian and slawsonite gels; see above) increase with increasing temperature in the Synpel glasses. Both Cs and Rb were added to melt by reaction of the starting biotite with temperature. Concentrations of Cs_2O in melt decrease with temperature as Cs is liberated with first melting and is then progressively diluted. Concentrations of Rb_2O increase slightly with increasing temperature as the crystalline phases that harbor Rb melt. Concentrations of F in all Synpel melts, contributed by reactions involving both muscovite and biotite, vary from 1.6 to 2.2 wt%. Concentrations of P_2O_5 vary between 0.09 and 0.16 wt%.

In summary, the compositions of the Synpel glasses correspond to evolved, F-rich, peraluminous leucogranites with the exception of the LILEs, the concentrations of which were artificially high to facilitate analysis (although the crystal-core reservoir effect noted above drops Ba and Sr contents of the system substantially). The melting of muscovite is more congruent than might have been expected (cf. Storre and Karotke 1971), and consequently melts are strongly peraluminous with ASI values near 1.4. At 200 MPa, the melts contain approximately 8 wt% H_2O at saturation (by difference from EMPA and Li from SIMS).

Feldspar

Compositions of feldspar rims are tabulated in Table 4. BSE imaging reveals that most feldspars, except for those in 650 °C reverse experiments, are compositionally zoned from core to rim.

The feldspars are stoichiometric, as illustrated in Figure 3, in which the sum of the alkalis (K, Na, Rb, and Cs) and silica are plotted against the sum of the alkaline earths (Ca, Sr, and Ba) and Al. The data define a straight line with a slope of −1, as expected. On a major element basis, conjugate forward- and reverse-direction experiments to 700 °C (6 + 7 and 6 + 3, for example) display nearly identical feldspar compositions: $Ab_{56.2}Or_{14.2}An_{16.4}$ vs. $Ab_{55.5}Or_{13.2}An_{16.1}$, respectively.

Digital X-ray maps, such as Figure 4, illustrate the distribution of elements within zoned feldspar crystals. Figures 4A and 4G display a BSE micrograph of a typical alkali feldspar with correlation between zoning and average atomic number. Figures 4D and 4J show that Ca is concentrated along the rim of a typical alkali feldspar from the Synpel experiments. Figures 4F, 4K, and 4L illustrate that both Ba and Sr are concentrated in the core (which is K-rich) and show no correlation with Ca. This relationship, Ba and Sr following K in feldspars, is illustrated quantitatively in Figure 5A. When the charge-balancing cations Al and Si are considered, substitution of Sr and Ba into feldspar rims appears to be governed by the simple exchange (Fig. 5B)

$$(Ba^{2+}, Sr^{2+}) + K^+ + Al^{3+} = 2Na^+ + Si^{4+} \quad (4)$$

TABLE 4. Feldspar compositions

Expt.	5 + 15	5 + 14	5 + 8	5 + 7	5 + 5	5 + 9	6 + 6
T (°C)	650, R	650, R	650, R	700, R	700, F	700, F	650, R
No. analyses	$n = 9$	$n = 13$	$n = 11$	$n = 7$	$n = 12$	$n = 10$	$n = 15$
SiO_2	57.29(0.40)	57.66(0.18)	58.83(0.26)	57.99(0.30)	56.69(0.20)	55.57(0.21)	59.70(0.46)
Al_2O_3	25.12(0.08)	24.58(0.21)	24.79(0.10)	22.39(0.36)	22.53(0.16)	26.09(0.09)	24.35(0.17)
MgO	00.09(0.07)	00.02(0.01)	00.02(0.02)	00.05(0.03)	*00.02*	*00.02*	*00.02*
CaO	04.11(0.18)	03.57(0.25)	04.42(0.11)	00.90(0.26)	00.66(0.09)	04.82(0.09)	03.83(0.10)
FeO	00.47(0.26)	00.21(0.03)	00.25(0.08)	00.28(0.08)	00.13(0.01)	00.18(0.02)	00.11(0.01)
SrO	03.58(0.15)	03.86(0.14)	03.30(0.10)	04.52(0.24)	05.59(0.30)	05.50(0.14)	01.97(0.22)
BaO	00.34(0.06)	00.51(0.07)	00.26(0.03)	03.53(0.40)	03.40(0.19)	00.09(0.06)	00.50(0.08)
Na_2O	06.16(0.10)	05.78(0.15)	06.30(0.03)	02.62(0.22)	02.61(0.11)	05.03(0.07)	07.44(0.17)
K_2O	01.82(0.20)	02.77(0.40)	01.58(0.13)	06.98(0.47)	07.44(0.28)	01.54(0.08)	01.30(0.10)
Rb_2O	*00.05*	00.05(0.02)	*00.05*	00.29(0.03)	00.26(0.02)	*00.05*	*00.05*
Cs_2O	*00.11*	*00.11*	*00.11*	00.11(0.03)	*00.11*	*00.11*	*00.11*
P_2O_5	00.07(0.01)	00.08(0.01)	00.09(0.01)	00.03(0.01)	*00.03*	00.07(0.01)	00.10(0.01)
Total	99.21	99.20	100.00	99.69	99.47	99.07	99.48
				Cations on 32 O atoms			
Si	10.58	10.69	10.72	11.05	10.93	10.36	10.85
Al	05.47	05.37	05.33	05.03	05.12	05.73	05.22
Mg	00.02	00.01	00.00	00.01	00.00	00.00	00.00
Ca	00.81	00.71	00.86	00.18	00.14	00.96	00.75
Fe	00.07	00.03	00.04	00.04	00.02	00.03	00.02
Sr	00.38	00.41	00.35	00.50	00.62	00.59	00.21
Ba	00.02	00.04	00.02	00.26	00.26	00.01	00.04
Na	02.21	02.08	02.23	00.97	00.98	01.82	02.62
K	00.43	00.66	00.37	01.70	01.83	00.37	00.30
Rb	00.00	00.01	00.00	00.04	00.03	00.00	00.00
Cs	00.00	00.00	00.00	00.01	00.00	00.00	00.00
P	00.01	00.01	00.01	00.00	00.00	00.01	00.02
Total	20.00	20.02	19.93	19.79	19.93	19.88	20.03
				Mol%			
Ab	57.21	53.27	58.22	26.48	25.30	48.51	67.01
Or	11.12	16.80	09.61	46.41	47.46	09.77	07.70
An	21.09	18.18	22.57	05.03	03.54	25.69	19.06
Slw	09.94	10.64	09.12	13.66	16.21	15.86	05.31
Cn	00.64	00.95	00.49	07.21	06.66	00.17	00.91
Rbf	00.00	00.15	00.00	00.97	00.84	00.00	00.00
Csf	00.00	00.00	00.00	00.24	00.00	00.00	00.00

Note: F = forward-direction experiment, R = reverse-direction experiment, Slw = slawsonite ($SrAl_2Si_2O_8$), Cn = celsian ($BaAl_2Si_2O_8$), Rbf = rubidium feldspar ($RbAlSi_3O_8$), Csf = cesium "feldspar" ($CsAlSi_3O_8$, see text). Numbers in italics represent detection limits.

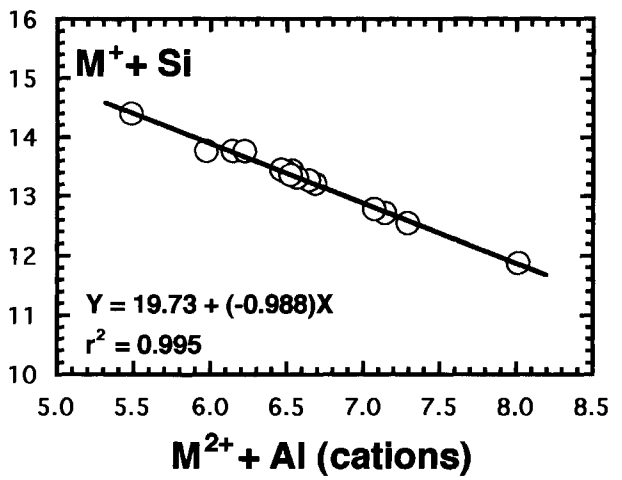

FIGURE 3. Plot of M^+ (=K, Na, Rb, and Cs) + Si^{4+} vs. M^{2+} (=Ca, Ba, and Sr) + Al^{3+} (cations) in feldspar rims. The least-squares-fitted line regressed through the data has a slope of nearly −1 and a correlation coefficient (r^2) of 0.995.

which is a linear combination of the exchanges

$$(Ba^{2+}, Sr^{2+}) + Al^{3+} = Na^+ + Si^{4+} \quad (5)$$

and

$$K^+ = Na^+. \quad (6)$$

These data suggest that SrO and BaO partition more strongly into orthoclase-rich feldspars than albite- and anorthite-rich feldspars.

Feldspar-melt partition coefficients

We determined empirical partition coefficients by dividing the concentration of the element of interest in feldspar by its concentration in glass. Following the recommendations of Beattie et al. (1993), this concentration ratio is denoted as

$$D(M)^{Fsp/gl} \quad (7)$$

where D, M, Fsp, and gl represent the distribution coefficient, the element of interest, feldspar, and glass, re-

TABLE 4.—*Continued*

Expt.	6 + 5	6 + 7	6 + 4	7 + 6	7 + 5	7 + 7	7 + 4
T (°C)	700, R	700, R	750, F	650, R	700, R	700, F	750, F
No. analyses	*n* = 17	*n* = 22	*n* = 18	*n* = 15	*n* = 11	*n* = 13	*n* = 15
SiO_2	59.05(0.15)	56.94(0.12)	55.65(0.14)	57.32(0.23)	58.35(0.35)	53.69(0.12)	55.46(0.19)
Al_2O_3	24.92(0.08)	24.74(0.13)	25.30(0.13)	26.50(0.12)	21.20(0.14)	27.73(0.10)	23.15(0.14)
MgO	*00.02*	00.04(0.02)	00.04(0.02)	00.06(0.05)	00.06(0.02)	*00.02*	*00.02*
CaO	04.25(0.08)	03.11(0.20)	03.03(0.20)	06.32(0.13)	00.24(0.02)	06.84(0.12)	00.66(0.05)
FeO	00.15(0.01)	00.24(0.06)	00.26(0.06)	00.30(0.15)	00.35(0.11)	00.17(0.01)	00.15(0.02)
SrO	02.93(0.06)	04.38(0.13)	06.22(0.15)	02.19(0.10)	02.96(0.16)	04.93(0.13)	06.56(0.25)
BaO	00.60(0.03)	01.55(0.15)	02.44(0.19)	00.16(0.03)	03.86(0.19)	00.55(0.02)	03.62(0.13)
Na_2O	06.63(0.03)	05.94(0.09)	04.81(0.08)	05.75(0.07)	01.50(0.02)	04.48(0.03)	01.65(0.04)
K_2O	01.28(0.05)	02.15(0.17)	02.47(0.13)	01.29(0.17)	10.38(0.20)	01.12(0.04)	08.23(0.15)
Rb_2O	*00.05*	*00.05*	*00.05*	*00.05*	00.47(0.03)	*00.05*	00.21(0.02)
Cs_2O	*00.11*	*00.11*	*00.11*	*00.11*	*00.11*	*00.11*	*00.11*
P_2O_5	*00.03*	00.04(0.00)	*00.03*	00.10(0.01)	00.04(0.01)	00.11(0.01)	*00.03*
Total	100.02	99.29	100.41	100.15	99.52	99.80	99.85
			Cations on 32 O atoms				
Si	10.73	10.62	10.45	10.40	11.23	09.99	10.77
Al	05.34	05.44	05.60	05.67	04.81	06.08	05.30
Mg	00.00	00.01	00.01	00.02	00.02	00.00	00.00
Ca	00.83	00.62	00.61	01.23	00.05	01.36	00.14
Fe	00.02	00.04	00.04	00.05	00.06	00.03	00.02
Sr	00.31	00.47	00.68	00.23	00.33	00.53	00.74
Ba	00.04	00.11	00.18	00.01	00.29	00.04	00.28
Na	02.34	02.15	01.75	02.02	00.56	01.62	00.62
K	00.30	00.51	00.59	00.30	02.55	00.27	02.04
Rb	00.00	00.00	00.00	00.00	00.06	00.00	00.03
Cs	00.00	00.00	00.00	00.00	00.00	00.00	00.00
P	00.00	00.01	00.00	00.02	00.01	00.02	00.00
Total	19.91	19.98	19.91	19.95	19.97	19.94	19.94
			Mol%				
Ab	61.28	55.53	45.97	53.35	14.59	42.33	16.19
Or	07.79	13.23	15.53	07.87	66.42	06.96	53.13
An	21.71	16.07	16.00	32.40	01.29	35.72	03.58
Slw	08.10	12.25	17.78	06.08	08.61	13.93	19.25
Cn	01.12	02.93	04.71	00.30	07.59	01.05	07.18
Rbf	00.00	00.00	00.00	00.00	01.52	00.00	00.68
Csf	00.00	00.00	00.00	00.00	00.00	00.00	00.00

spectively. Partition coefficients determined in this study are listed in Table 5.

Sr. Values of $D(Sr)^{Fsp/gl}$ vary between ~9 and 23. The spread of values could be due, in part, to analytical problems in determining Sr (note the background problem discussed in the Appendix of Icenhower and London 1995). To assess this possibility, in Figure 6A we plotted concentrations of SrO in glass vs. SrO in feldspar with compositions grouped according to temperature history. This figure illustrates that the data, as a whole, form a linear array and that forward-direction experiments to 700–750 °C form a relatively tight cluster in comparison with the reverse-direction experiments. We interpret these data to indicate that reverse-direction experiments probably did not attain equilibrium in all cases.

Blundy and Wood (1991) suggested that the partitioning of Sr between plagioclase and melt is governed by the mole fraction of the albite component in feldspar. Figure 6B is a plot of $D(Sr)^{Fsp/gl}$ vs. albite contents of feldspar crystals for the Synpel experiments; the values of the partition coefficients show no obvious trend with feldspar composition. A plot of the sum of orthoclase and albite against $D(Sr)^{Fsp/gl}$ shows that orthoclase content of feldspar has no discernible impact on the distribution of Sr between feldspar and melt (Fig. 6C). We therefore conclude that $D(Sr)^{Fsp/gl}$ is independent of alkali feldspar composition.

Ba. Values of $D(Ba)^{Fsp/gl}$ vary between ~1 and 19, closely corresponding to the range of values reported in the literature (cf. Henderson 1982). The correlation of Ba with K described above can also be seen in a plot of the orthoclase content of feldspar (in mole percent) with $D(Ba)^{Fsp/gl}$ (Fig. 7A). The linear fit over the range of orthoclase contents, from ~5 to 70 mol%, has a correlation coefficient (r^2, deviation about the means) of 0.984 with an intercept of 0.07. This low intercept value is significant because low orthoclase contents correspond to plagioclase compositions that have reported $D(Ba)^{Fsp/gl}$ values of <1 (cf. Henderson 1982). From these experiments, the equation

$$D(Ba)^{Fsp/gl} = 0.07 + (0.25)\text{orthoclase} \quad (8)$$

describes the distribution of Ba between feldspar and melt. The range of Ba partition coefficients reported in this pa-

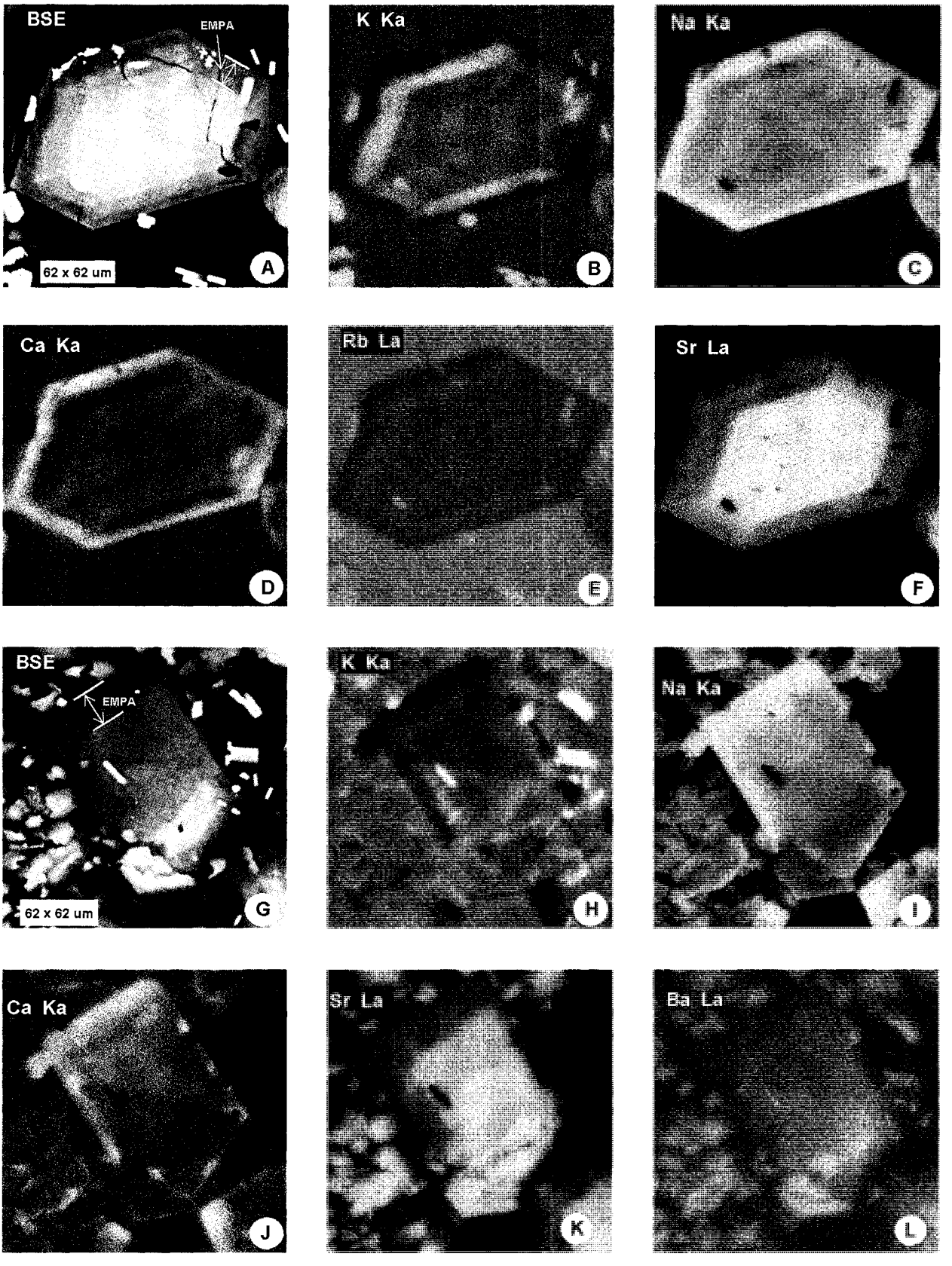
BSE
EMPA
62 x 62 um
A
K Ka
B
Na Ka
C
Ca Ka
D
Rb La
E
Sr La
F
BSE
EMPA
62 x 62 um
G
K Ka
H
Na Ka
I
Ca Ka
J
Sr La
K
Ba La
L

per, ~1 to 20, spans the range of values reported in the literature, from ~1 to 22 (e.g., Henderson 1982; Jolliff et al. 1992). We therefore suggest that the range of partition-coefficient values reported in the literature are real and that they reflect variable orthoclase content of the alkali feldspar crystals.

Rb and Cs. Our experimental results (Table 5) indicate that $D(\mathrm{Rb})^{\mathrm{Fsp/gl}}$ values are all <1 for the feldspar compositions studied. Rb partition coefficients also appear to be related to the orthoclase content of feldspars. When $D(\mathrm{Rb})^{\mathrm{Fsp/gl}}$ is plotted against orthoclase (Fig. 7B), a least-squares fit for a line regressed through the data yields a correlation coefficient of 0.927 and an intercept of 0.03. The low intercept value, corresponding to albitic plagioclase compositions, is similar to the low $D(\mathrm{Rb})^{\mathrm{Fsp/gl}}$ values reported for plagioclases in intermediate to rhyolitic systems (e.g., Henderson 1982). The equation that describes Rb partitioning is

$$D(\mathrm{Rb})^{\mathrm{Fsp/gl}} = 0.03 + (0.01)\mathrm{orthoclase}. \quad (9)$$

Note that near pure orthoclase, Equation 8 predicts that $D(\mathrm{Rb})^{\mathrm{Fsp/gl}}$ should slightly exceed unity, which conforms to the values reported by other investigators (0.3–1.3) for potassium feldspar phenocrysts separated from volcanic rocks (e.g., Henderson 1982; Jolliff et al. 1992). We propose that the range of values reported in the literature also correlate with variable orthoclase content of the alkali feldspar phenocrysts, with only a few exceptions. [For example, Nash and Crecraft (1985) determined values of $D(\mathrm{Rb})^{\mathrm{Fsp/gl}}$ between 1 and 3.]

Because Cs_2O concentrations are below detection level in all but one feldspar rim, only one significant value of $D(\mathrm{Cs})^{\mathrm{Fsp/gl}}$ can be reported. The low value (0.13) from a relatively orthoclase-rich feldspar is in line with the low values proposed by other investigators (e.g., 0.14: Jolliff et al. 1992).

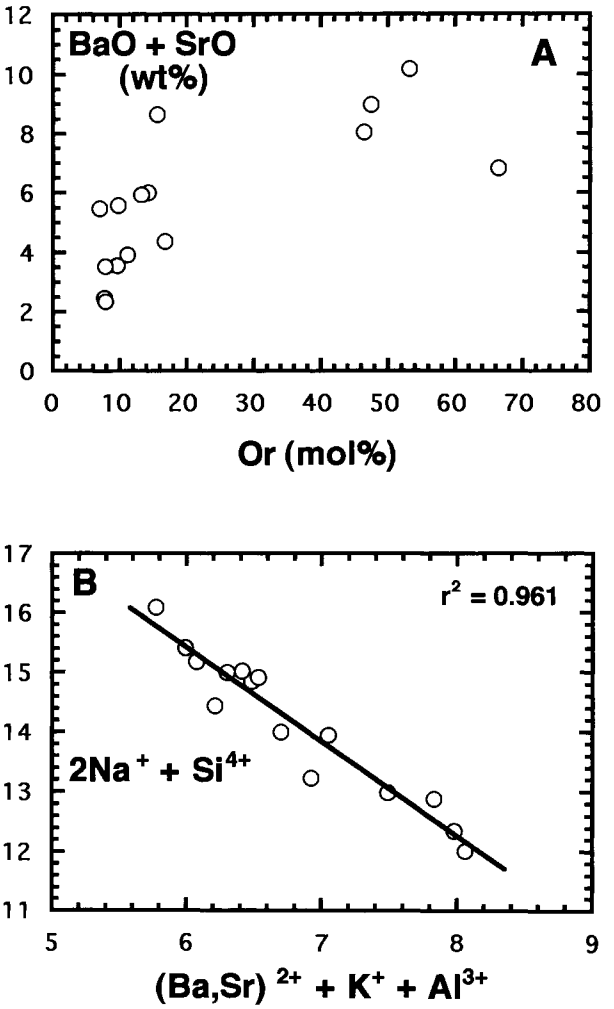

FIGURE 5. (A) Plot of BaO + SrO vs. orthoclase in feldspar rims. The general trend of the data is toward increasing Ba and Sr with K. (B). Plot of $2Na^+ + Si^{4+}$ vs. $(Ba, Sr)^{2+} + K^+ + Al^{3+}$ (cations) in feldspar rims. The least-squares-fitted line regressed through the data has a correlation coefficient (r^2) of 0.961. The data are consistent with Ba and Sr following K into feldspar.

DISCUSSION

Partition coefficients

Our values of partition coefficients for Sr between feldspar and melt range from 8 to 23. We speculate that some of the scatter of values is due to the failure of Sr distributions to reach equilibrium in reversed experiments, though the other elements (e.g., Ba) show no such scatter; the other potential source of error, which we do not believe is applicable, is a variation in continuum radiation on the high 2θ side of the Sr$K\alpha$ X-ray line, where we selected our background counting position. We note that in the experimental study by Long (1978), values of $D(\mathrm{Sr})^{\mathrm{Fsp/gl}}$ also showed the widest scatter of all LILEs studied.

The values of $D(\mathrm{Sr})^{\mathrm{Fsp/gl}}$ in our forward-direction experiments, 10–14, are similar to those obtained from nat-

←

FIGURE 4. Digital back-scattered electron (BSE) and X-ray images of two alkali feldspars in Synpel experiments. The BSE images, **A** and **G**, illustrate complex zonation typical of all the experimental products. The regions of **A** and **G** marked "EMPA" are representative of the feldspar rims from which electron microprobe analyses were collected for this study. X-ray maps show a clear inverse zonation of K, Na, and Ca, with more Na-Ca–rich rims surrounding K-richer interiors of cores. Cores are rich in Ba and Sr (major components) to the exclusion of K, Na, and Ca; as trace elements, however, Rb, Ba, and Sr correlate positively with K (e.g., compare **B** and **E**) and inversely with plagioclase components (e.g., compare **I** and **J** vs. **K**).

TABLE 5. Apparent partition coefficients

Expt.	5 + 15	5 + 14	5 + 8	5 + 7	5 + 5	5 + 9	6 + 6	6 + 5
T (°C)	650, R	650, R	650, R	700, R	700, F	700, F	650, R	700, R
SiO_2	00.90(0.01)	00.90(0.00)	00.89(0.00)	00.91(0.01)	00.89(0.00)	00.88(0.00)	00.91(0.01)	00.94(0.00)
Al_2O_3	01.59(0.01)	01.57(0.02)	01.59(0.01)	01.32(0.02)	01.33(0.01)	01.57(0.01)	01.50(0.01)	01.44(0.01)
MgO	00.56(0.44)	00.18(0.10)	00.20(0.15)	00.38(0.23)	<00.34	<00.27	<00.40	<00.34
CaO	04.95(0.22)	04.35(0.31)	05.53(0.19)	00.96(0.28)	00.65(0.09)	05.42(0.14)	08.70(0.28)	06.97(0.18)
FeO	00.64(0.35)	00.33(0.05)	00.41(0.13)	00.38(0.12)	00.21(0.01)	00.27(0.04)	00.28(0.03)	00.28(0.03)
SrO	07.96(0.72)	18.38(2.71)	15.00(1.32)	10.51(1.59)	13.98(0.95)	13.41(1.19)	17.91(2.80)	09.16(0.82)
BaO	01.26(0.27)	02.43(0.57)	01.18(0.17)	11.03(1.76)	12.59(0.97)	02.93(0.27)	04.55(0.86)	02.61(0.24)
Na_2O	03.16(0.06)	03.75(0.20)	02.88(0.03)	01.29(0.13)	01.13(0.05)	02.55(0.09)	02.63(0.06)	02.31(0.02)
K_2O	00.55(0.06)	00.88(0.13)	00.48(0.04)	01.85(0.13)	01.93(0.07)	00.45(0.02)	00.40(0.03)	00.37(0.01)
Rb_2O	<00.08	00.09(0.04)	<00.08	00.45(0.05)	00.38(0.03)	<00.09	<00.07	<00.08
Cs_2O	<00.11	<00.10	<00.10	00.13(0.04)	<00.11	<00.12	<00.10	<00.11
P_2O_5	00.58(0.03)	00.67(0.10)	00.63(0.09)	00.23(0.08)	<00.26	00.52(0.06)	00.73(0.08)	<00.27

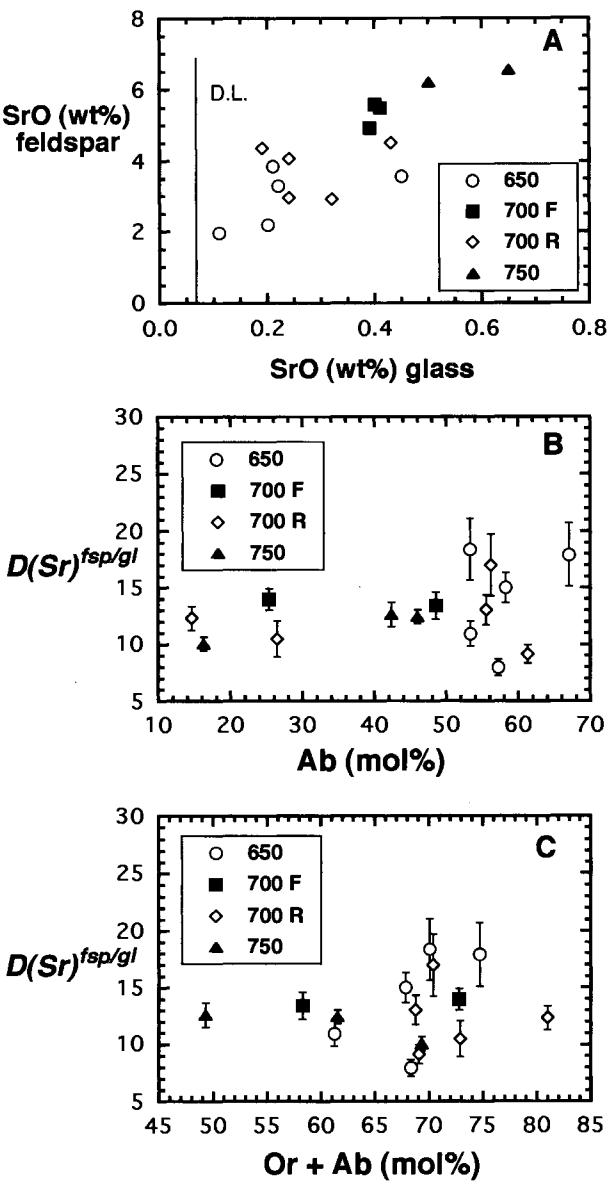

ural albite-rich plagioclase (Blundy and Wood 1991). These investigators attributed the preferential distribution of Sr into albite-rich over anorthite-rich plagioclase to a more open or "elastic" crystalline structure of the former. Because orthoclase and albite have similar densities and are both less dense than anorthite (Deer et al. 1966) we expect that Sr also partitions in favor of orthoclase-rich over anorthite-rich anorthoclase. It is clear, however, that variations in albite and orthoclase contents in alkali feldspar crystals do not affect partitioning behavior of Sr.

Incorporation of Ba into alkali feldspar is a linear function of the orthoclase content. Though the operative exchange is $BaAlM^{\pm}{}_1Si_{-1}$, Ba is incompatible in the denser structure of calcic plagioclase (Deer et al. 1966; see also Blundy and Wood 1991), but compatible in potassium feldspar. In these experiments, however, the thermal stability of the celsian (Cn) component is similar to that of calcic plagioclase. Therefore, Cn-rich alkali feldspar is the first feldspar to form at highest temperatures, and its crystallization removes K from melt (i.e., K acts as a trace rather than major element). Upon cooling, the feldspars become more sodic and hence display reverse zonation, with Ba (K, Rb, Sr)-rich cores and Na (Ca)-richer rims (from which EMPA were obtained). In a sense, the result is a Rapakivi feldspar (e.g., Fig. 4), formed by the high thermal stability of the Cn component, which pulls K from melt as the alkali feldspar crystallizes.

←

FIGURE 6. (A) Concentration of SrO in feldspar vs. SrO in glass. The data are grouped according to temperature history and illustrate a general positive trend. Note that the forward-direction experiments are tightly grouped. (B) Plot of $D(Sr)^{Fsp/gl}$ vs. albite in feldspar. Error bars represent 1σ uncertainty on the basis of multiple experiments and counting statistics (see Appendix of Icenhower and London 1995). (C) Plot of $D(Sr)^{Fsp/gl}$ vs. orthoclase + albite in feldspar. The data indicate no correlation between the two parameters (see text).

TABLE 5.—*Continued*

Expt.	6 + 3	6 + 7	6 + 4	7 + 6	7 + 5	7 + 7	7 + 4
T (°C)	700, R	700, R	750, F	650, R	700, R	700, F	750, F
SiO_2	00.92(0.00)	00.91(0.00)	00.91(0.00)	00.89(0.00)	00.93(0.01)	00.87(0.00)	00.91(0.00)
Al_2O_3	01.37(0.01)	01.42(0.01)	01.38(0.01)	01.62(0.01)	01.24(0.01)	01.60(0.01)	01.25(0.01)
MgO	<00.20	00.57(0.29)	00.33(0.18)	00.75(0.66)	00.55(0.23)	<00.30	<00.24
CaO	04.57(0.30)	05.10(0.33)	03.99(0.27)	06.58(0.15)	00.21(0.02)	06.98(0.14)	00.65(0.05)
FeO	00.27(0.04)	00.38(0.09)	00.31(0.07)	00.57(0.29)	00.52(0.16)	00.25(0.01)	00.18(0.02)
SrO	17.00(2.73)	23.05(1.29)	12.44(0.59)	10.95(1.10)	12.33(1.04)	12.64(1.08)	10.09(0.60)
BaO	04.18(0.56)	06.20(0.66)	05.42(0.45)	01.07(0.27)	18.38(1.45)	02.89(0.41)	12.93(0.95)
Na_2O	02.09(0.07)	02.29(0.09)	01.84(0.07)	03.13(0.08)	00.72(0.01)	02.45(0.04)	00.96(0.05)
K_2O	00.64(0.06)	00.63(0.05)	00.68(0.04)	00.37(0.05)	02.47(0.05)	00.30(0.01)	01.68(0.04)
Rb_2O	<00.07	<00.08	<00.08	<00.08	00.76(0.05)	<00.08	00.31(0.03)
Cs_2O	<00.11	<00.12	<00.12	<00.09	<00.10	<00.10	<00.11
P_2O_5	<00.24	00.31(0.08)	<00.29	01.16(0.12)	00.31(0.06)	00.69(0.06)	<00.22

Carron and Lagache (1980) argued that partitioning of LILEs is controlled by melt composition, as indexed by K/(K + Na). Figure 8 illustrates that partitioning of Sr and Ba is not controlled by K′ of melt [$100K_2O/(\Sigma$ alkali oxides + Σ alkaline earth oxides)].

Though a large cation, Rb is yet small enough to be compatible in the structure of orthoclase-rich alkali feldspar. The larger size of Cs is clearly incompatible with alkali feldspar structures. Although micas may accommodate appreciable Cs in the interlayer site (e.g., the Tanco biotite used as starting material here), Rb and Cs are generally incompatible in all rock-forming minerals. Cs does approach compatible behavior in structural channels, as in cordierite [$D(Cs)^{Crd/gl} = 0.8$, Icenhower et al. 1994] and possibly beryl (Deer et al. 1966).

Comparison with natural rocks

Partition-coefficient data determined on volcanic rocks collectively show some intriguing similarities to our results. The data show a positive correlation among $D(Rb)^{Fsp/melt}$, $D(Ba)^{Fsp/melt}$, and orthoclase content of feldspar (Fig. 9). We find it significant that most of the data overlap despite differences in melt composition and temperature. Both Figures 9A and 9B show that several data sets are consistent with our results. For example, values of $D(Ba)^{Fsp/melt}$ determined by Nash and Crecraft (1985) and a set of data tabulated by Smith and Brown (1988) are reasonably similar to our results; values reported by Leeman and Phelps (1981) and Piccirillo et al. (1975) display scattering and are, on the whole, not consistent with the rest of the data. Values of $D(Rb)^{Fsp/melt}$ reported by Drexler et al. (1983), Wörner et al. (1983), Hildreth (1980), Mahood and Hildreth (1983), Kovalenko et al. (1981), and Leeman and Phelps (1981) are all in reasonable accord with our data. However, the values of $D(Rb)^{Fsp/melt}$ reported by Nash and Crecraft (1985) are not consistent with these data. We conclude from this that melt composition and temperature are likely second-order effects on Ba and Rb partition coefficients. Our data are consistent with the bulk of values determined by oth-

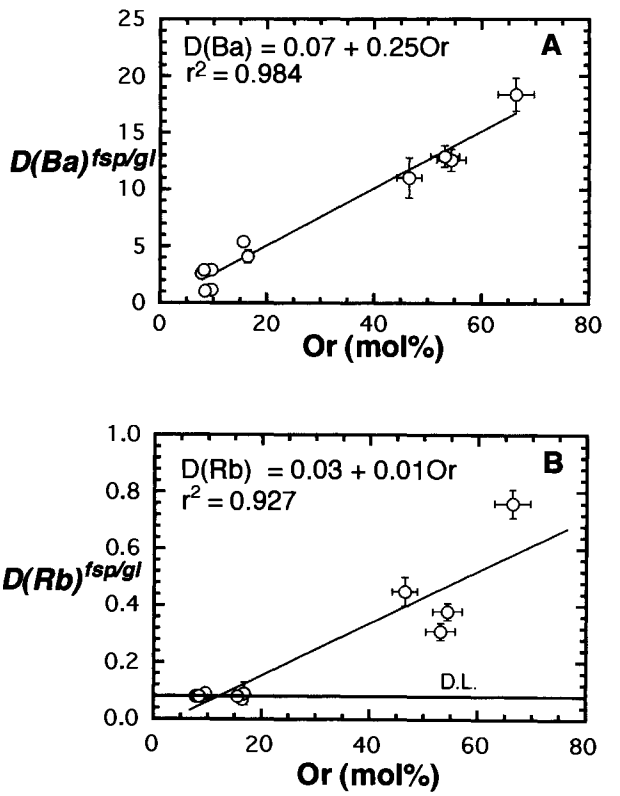

FIGURE 7. (**A**) Plot of $D(Ba)^{Fsp/gl}$ vs. orthoclase feldspar. The least-squares-fitted line regressed through the data has a slope of 0.25, an intercept of 0.07, and a correlation coefficient (r^2) of 0.984. (**B**) Plot of $D(Rb)^{Fsp/gl}$ vs. orthoclase feldspar. The least-squares-fitted line regressed through the data has a slope of 0.01, an intercept of 0.03, and a correlation coefficient (r^2) of 0.927. D.L. stands for the detection limit; glass contains detectable Rb but is below detection for feldspar (0.05 wt%). Therefore, values of $D(Rb)^{Fsp/gl}$ are <0.09. Note that the error bars for some data are smaller than the symbol.

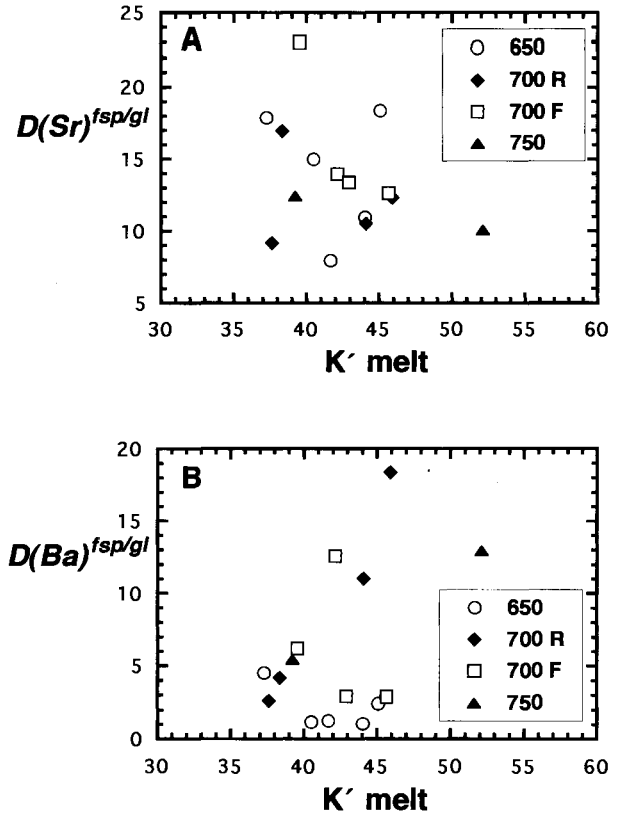

FIGURE 8. (A) Plot of $D(Sr)^{Fsp/gl}$ and (B) $D(Ba)^{Fsp/gl}$ vs. K′ [= $100K_2O/(\Sigma$ alkali oxides + Σ alkaline earth oxides)] in glass. We suggest that Sr and Ba partitioning shows no correlation with K′ in melt.

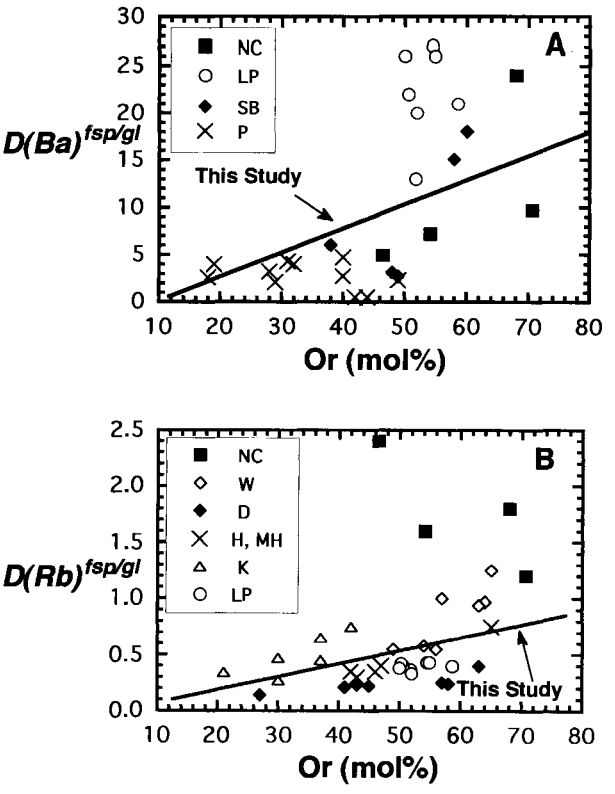

FIGURE 9. (A) Plot of $D(Ba)^{Fsp/gl}$ vs. orthoclase for potassium feldspar–matrix pairs in natural volcanic rocks. Our data are represented by the straight line (see Fig. 7). Sources include: NC = Nash and Crecraft (1985), LP = Leeman and Phelps (1981), SB = Smith and Brown (1988), and P = Piccirillo et al. (1975). (B) Plot of $D(Rb)^{Fsp/gl}$ vs. orthoclase for potassium feldspar–matrix pairs in natural volcanic rocks. Our data are represented by the straight line (see Fig. 7). Sources include: NC = Nash and Crecraft (1985), W = Wörner et al. (1983), D = Drexler et al. (1983), H and MH = Hildreth (1980) and Mahood and Hildreth (1983), K = Kovalenko et al. (1981), and LP = Leeman and Phelps (1981).

er investigators and have the advantage of quantifying the relationship between feldspar composition and partition coefficients; previous individual data sets have not been able to make this quantification.

LILE signatures of S-type melts

At anatexis. Aluminous metasediments at conditions of the amphibolite facies contain assemblages that include muscovite + biotite + quartz + aluminum silicate and sodic plagioclase or ternary feldspar, with the micas constituting the primary sources of Li, Rb, Cs, and Ba. Because ternary feldspar compositions are sodic, values of $D(Ba)^{Fsp/melt}$ would be small at the inception of melting. However, the bulk distribution coefficient for Ba [$D(Ba)^{bulk}$] remains high because of the compatibility of Ba in biotite (Icenhower and London 1995) and increases as orthoclase-rich alkali feldspar is generated by Reaction 2 or 3. The maximum amount of Ba that an S-type melt can obtain during medium-pressure (400–600 MPa) anatexis, therefore, may be highest at the inception of melting but decreases as orthoclase-rich alkali feldspar is produced from mica breakdown. Given the relatively low partition coefficients for Rb between micas and melt [$D(Rb)^{Bt/melt} = 2$, $D(Rb)^{Ms/melt} = 1.6$: Icenhower and London 1995] and the generally incompatible behavior of Rb in alkali feldspar, the solid assemblage above the peritectic would have to be made up of >50 wt% micas for $D(Rb)^{bulk}$ to become >1. It seems likely, therefore, that Rb behaves as an incompatible element (cf. Harris and Inger 1992). Both Li [$D(Li)^{Bt/melt} = 1.7$–1.0, $D(Li)^{Ms/melt} = 0.8$] and Cs [$D(Cs)^{Bt/melt} = 0.4$, $D(Cs)^{Ms/melt} = 0.3$] are partitioned into melt over likely residual phases (Icenhower and London 1995). Cordierite, if present, is a source or sink for Cs (Icenhower et al. 1994) depending on its participation in melting reactions (Icenhower 1995; Icenhower and London, in preparation). Albite or the albite component of plagioclase also melts in large proportion at the peritectic minimum and constitutes a source of Sr.

At pressures above the invariant point I_1 in Figure 1, muscovite survives above the melting peritectic if it con-

stitutes >20 wt% of the rock, which is the normative muscovite component of the minimum melt composition. For less micaceous rocks, melt compositions evolve with increasing T toward less aluminous, more sodic compositions as residual sodic feldspar (a component of plagioclase or alkali feldspar) dominates the melting reaction. With this trend, orthoclase-rich alkali feldspar is not produced in abundance at temperatures above the liquidus, and consequently the LILE signature of melt is determined primarily by (1) the muscovite component added to melt at the minimum, (2) the reactions of biotite only with increasing T (see Icenhower and London 1995), and (3) for Sr, the continuous reaction of plagioclase toward anorthite-rich compositions (e.g., Blundy and Wood 1991). In contrast, very muscovite-rich schists can generate only a small fraction of melt because albite is a limiting component (Patiño Douce and Johnston 1991). In such a case, the higher T reaction of muscovite (Reaction 2 or 3) contributes a very large fraction of LILEs, especially Li and Cs, to a small fraction of melt, and Ba (and to a lesser extent Rb) is sequestered by orthoclase-rich alkali feldspar. Such a process, in which small degrees of partial melting are obtained from very micaceous rocks and muscovite breaks down to orthoclase-rich alkali feldspar by Reaction 2 or 3 above the solidus of the system, may explain how S-type magmas derive their LILE signature, which Cerny (1991) has termed the LCT family of rocks for their distinctively high concentrations of Li, Cs, and Ta.

Upon crystallization. With the data presented here on alkali feldspar, plus the data of similar partitioning experiments for biotite and muscovite (Icenhower and London 1995) and for plagioclase (e.g., Blundy and Wood 1991), it is now possible to model in detail the LILE fractionation in melt as a function of changing alkali feldspar, plagioclase, and mica compositions in addition to variations in temperature. Crystallization of feldspars typically has a dramatic impact on the concentrations of LILEs in residual melt, especially for peraluminous leucogranites, the simple chemistries of which dictate that copious feldspar must crystallize. As this study indicates, both Ba and Sr become severely depleted while Cs and Li increase dramatically, perhaps in melts that are already relatively enriched in these elements (see above). Concentrations of Rb also increase unless biotite or muscovite is a major component (>50 wt%) of the fractionating assemblage. Note that crystallization of micas has very little impact on the concentrations of Cs and Li in residual melt.

For the purposes of modeling either the source regions or the crystallization of granitic rocks, it is not adequate to select a particular partition coefficient for a LILE without consideration of the mineral composition. Among the LILEs, however, Cs is clearly the least compatible in the rock-forming minerals of micas and feldspars, followed by Li, Rb, and Ba. Conversely, the enthalpies of mixing among $M^{n+}_{1/n}AlO_2$-SiO_2 (M = Li, Na, K, Rb, Cs, Mg, Ca, Sr, Ba, Pb) components in melts become less negative in approximately this same sequence (Roy and Navrotsky 1984), which reflects the extent to which LILEs like Cs stabilize melt structures, whereas cations with higher field strengths such as Ba do not.

Acknowledgments

Financial support for this research was provided by NSF-EPSCoR contract EHR-9108771 to D.L. for collaborative research with the University of Tulsa. The Electron Microprobe Laboratory was created by grant DE-FG22-87FE1146 to D.L. from the U.S. Department of Energy, and the experimental facilities were established and maintained by grants EAR-8516753, EAR-8720498, and EAR-8821950 to D.L. from the National Science Foundation. We thank George Morgan for aid in microprobe analyses, and Roger Nielsen and an anonymous reviewer for comments that improved the manuscript.

References cited

Althaus, E., Karotke, E., Nitsch, K.H., and Winkler, H.G.F. (1970) An experimental re-examination of the upper stability limit of muscovite plus quartz. Neues Jahrbuch für Mineralogie Monatshefte, 325–336.

Anderson, J.L. (1983) Proterozoic anorogenic granite plutonism of North America. Geologic Society of America Memoir 161, 113–154.

Arth, J.G. (1976) Behavior of trace elements during magmatic processes: A summary of the theoretical models and their applications. U.S. Geological Survey Journal of Research, 4, 41–47.

Beattie, P., Drake, M., Jones, J., Leeman, W., Longhi, J., McKay, G., Nielsen, R., Palme, H., Shaw, D., Takahashi, E., and Watson, E.B. (1993) Terminology for trace-element partitioning. Geochimica et Cosmochimica Acta, 57, 1605–1606.

Berlin, R., and Henderson, C.M.B. (1969) The distribution of Sr and Ba between the alkali feldspar, plagioclase and groundmass phases of porphyritic trachytes and phonolites. Geochimica et Cosmochimica Acta, 33, 247–255.

Blundy, J.D., and Wood, B.J. (1991) Crystal-chemical controls on the partitioning of Sr and Ba between plagioclase feldspar, silicate melts, and hydrothermal solutions. Geochimica et Cosmochimica Acta, 55, 193–209.

Carmichael, I.S.E., and McDonald, A. (1961) The geochemistry of some natural acid glasses from the North Atlantic Tertiary volcanic province. Geochimica et Cosmochimica Acta, 25, 189–222.

Carron, J.-P., and Lagache, M. (1980) Étude expérimentale du fractionnement des éléments Rb, Cs, Sr et Ba entre feldspaths alcalins, solutions hydrothermales et liquides silicatés dans le système Q.Ab.Or.H_2O à 2 kbar entre 700 et 800 °C. Bulletin Minéralogy, 103, 571–578.

Cerny, P. (1991) Fertile granites of Precambrian rare-element pegmatite fields: Is geochemistry controlled by tectonic setting or source lithologies? Precambrian Research, 51, 429–468.

Deer, W.A., Howie, R.A., and Zussman, J. (1966) An introduction to the rock forming minerals, p. 1–528. Longman, London, U.K.

De Pieri, R., and Quareni, S. (1978) Partition coefficients of alkali and alkaline-earth elements between alkali feldspar phenocrysts and their lava matrix. Mineralogical Magazine, 42, 63–67.

Drake, M.J. (1972) The distribution of major and trace elements between plagioclase feldspar and magmatic silicate liquid: An experimental study. Ph.D. thesis, University of Oregon, Eugene.

Drexler, J.W., Bornhorst, T.J., and Noble, D.C. (1983) Trace-element sanidine/glass distribution coefficients for peralkaline silicic rocks and their implications to peralkaline petrogenesis. Lithos, 16, 265–271.

Ewart, A., and Taylor, S.R. (1969) Trace element geochemistry of the rhyolitic volcanic rocks, Central North Island, New Zealand: Phenocryst data. Contributions to Mineralogy and Petrology, 22, 127–146.

Green, T.H., and Pearson, N.J. (1983) Effect of pressure on rare earth element partition coefficients in common magmas. Nature, 305, 414–416.

Guo, J., and Green, T.H. (1989) Barium partitioning between alkali feldspar and silicate liquid at high temperature and pressure. Contributions to Mineralogy and Petrology, 102, 328–335.

Harris, N.B.W., and Inger, S. (1992) Trace element modelling of pelite-

derived granites. Contributions to Mineralogy and Petrology, 110, 46–56.
Hart, S.L., and Davis, K.E. (1978) Nickel partitioning between olivine and silicate melt. Earth and Planetary Science Letters, 40, 203–220.
Henderson, P. (1982) Inorganic geochemistry, p. 3–353. Pergamon, Oxford, U.K.
Higuchi, H., and Nagasawa, H. (1969) Partition of trace elements between rock-forming minerals and the host volcanic rocks. Earth and Planetary Science Letters, 7, 281–287.
Hildreth, W. (1980) The Bishop Tuff: Evidence for the origin of compositional zonation in silicic magma chambers. Geological Society of America Special Paper 180, 43–75.
Hogan, J.P., and Sinha, A.K. (1991) The effect of accessory minerals on the redistribution of lead isotopes during crustal anatexis: A model. Geochimica et Cosmochimica Acta, 55, 335–348.
Icenhower, J.P. (1995) Experimental determination of element behavior in silicic systems during hydrous partial fusion, 227 p. Ph.D. dissertation, University of Oklahoma, Norman.
Icenhower, J.P., and London, D. (1993a) Experimentally determined partitioning of Ba and Rb between alkali feldspar, biotite, muscovite, and peraluminous silicic melt. Eos, 74(16), 342.
——— (1993b) Experimental anatexis and trace-element behavior in the system Qtz − Ab − Mu ± Bt ± Als at 200 MPa (H_2O). Eos, 74(16), 343.
Icenhower, J.P., London, D., and Layne, G.D. (1994) Element partitioning among biotite, muscovite, garnet, cordierite, and peraluminous melt: Behavior of Li and Mn. Geological Society of America Abstracts with Programs, 26, A-290.
Icenhower, J.P., and London, D. (1995) An experimental study of element partitioning among biotite, muscovite, and coexisting peraluminous granitic melt at 200 MPa (H_2O). American Mineralogist, 80, 1229–1251.
Jolliff, B.L., Papike, J.J., and Shearer, C.K. (1992) Petrogenetic relationships between pegmatite and granite based on geochemistry of muscovite in pegmatite wall zones, Black Hills, South Dakota, USA. Geochimica et Cosmochimica Acta, 56, 1915–1939.
Kovalenko, V.I., Antipin, V.S., Ryabchikov, I.D., and Petrov, L.L. (1981) Variations in the rubidium distribution coefficient in igneous rocks. Geochemistry International, 21, 66–84.
Leeman, W.P., and Phelps, D.W. (1981) Partitioning of rare earths and other trace elements between sanidine and coexisting volcanic glass. Journal of Geophysical Research, 86, 10193–10199.
Le Fort, P., Cuney, M., Deniel, C., France-Lanord, C., Sheppard, S.M.F., Upreti, B.N., and Vidal, P. (1987) Crustal generation of the Himalayan leucogranites. Tectonophysics, 134, 39–57.
London, D. (1992) The application of experimental petrology to the genesis and crystallization of granitic pegmatites. In Granitic pegmatites (R.F. Martin and P. Cerny, Eds.). Canadian Mineralogist, 30, 499–540.
Long, P.E. (1978) Experimental determination of partition coefficients for Rb, Sr, and Ba between alkali feldspar and silicate liquid. Geochimica et Cosmochimica Acta, 42, 833–846.
Mahood, G., and Hildreth, W. (1983) Large partition coefficients for trace elements in high-silica rhyolites. Geochimica et Cosmochimica Acta, 47, 11–30.
Matsui, A., Onuma, N., Nagasawa, H., Higuchi, H., and Banno, S. (1977) Crystal structure control in the trace element partition between crystal and magma. Bulletin le Societe France Mineral et Cristallografi, 100, 315–324.
Merrill, R.B., Robertson, J.K., and Wyllie, P.J. (1970) Melting reactions in the system $NaAlSi_3O_8$-$KAlSi_3O_8$-SiO_2-H_2O to 20 kilobars compared with results for the feldspar-quartz-H_2O and rock-H_2O systems. Journal of Geology, 78, 558–569.
Montel, J.M. (1986) Experimental determination of the solubility of Ce-monazite in SiO_2-Al_2O_3-K_2O-Na_2O melts at 800 °C, 2 kbar, under H_2O-saturated conditions. Geology, 14, 659–662.
Morgan, G.B.,VI, and London, D. (1987) Alteration of amphibolitic wallrocks around the Tanco rare-element pegmatite, Bernic Lake, Manitoba. American Mineralogist, 72, 1097–1121.
Mysen, B.O., and Virgo, D. (1980) Trace element partitioning and melt structure: An experimental study at 1 atm. pressure. Geochimica et Cosmochimica Acta, 44, 1917–1930.
Nagasawa, H., and Schnetzler, C.C. (1971) Partitioning of rare earth, alkali and alkaline earth elements between phenocrysts and acidic igneous magma. Geochimica et Cosmochimica Acta, 35, 953–968.
Nash, W.P., and Crecraft, H.R. (1985) Partition coefficients for trace elements in silicic magmas. Geochimica et Cosmochimica Acta, 49, 2309–2322.
Nielsen, R.L. (1988) A model for the simulation of the combined major and trace element liquid lines of descent. Geochimica et Cosmochimica Acta, 52, 27–38.
Patiño Douce, A.E., and Johnston, A.D. (1991) Phase equilibria and melt productivity in the pelitic system: Implications for the origin of peraluminous granitoids and aluminous granulites. Contributions to Mineralogy and Petrology, 107, 202–218.
Piccirillo, E.M., Gregnanin, A., and De Pieri, R. (1975) Le ignimbriti della formazione oligocenia di Alagi (Altopiano Etiopico Centrale). Atti Memorie Accad Paavina Sci Lett Arti 87 Part II, Sci Mat Nat, 51–90.
Pouchou, J.L., and Pichoir, J. (1984) A new model for quantitative X-ray microanalysis. Recher Aeropat, 3, 167–192.
Ragland, P.C. (1989) Basic analytical petrology, 369 p. Oxford University Press, New York.
Roy, B.N., and Navrotsky, A. (1984) Thermochemistry of charge coupled substitutions in silicate glasses: The systems $M^{n+}_{1/n}AlO_2$-SiO_2 (M = Li, Na, K, Rb, Cs, Mg, Ca, Sr, Ba, Pb). Journal of the American Ceramic Society, 67, 606–610.
Ryerson, F.J., and Hess, P.C. (1978) Implication of liquid-liquid distribution coefficients to mineral-liquid partitioning. Geochimica et Cosmochimica Acta, 42, 921–932.
Smith, J.V., and Brown, W.L. (1988) Feldspar minerals: I. Crystal structures, physical, chemical, and microtextural properties, 828 p. Springer-Verlag, Berlin.
Storre, B., and Karotke, E. (1971) An experimental determination of the upper stability limit of muscovite + quartz in the range 7–20 kb water pressure. Neues Jahrbuch für Mineralogie Monatshefte, 237–240.
Sun, C., Williams, R.J., and Sun, S.S. (1974) Distribution of coefficients of Eu and Sr for plagioclase-liquid and clinopyroxene-liquid in oceanic ridge basalt: An experimental study. Geochimica et Cosmochimica Acta, 38, 1415–1433.
Thompson, A.B., and Tracy, R.J. (1979) Model systems for anatexis of pelitic rocks: II. Facies series melting and reactions in the system CaO-$KAlO_2$-$NaAlO_2$-Al_2O_3-SiO_2-H_2O. Contributions to Mineralogy and Petrology, 70, 429–438.
Watson, E.B. (1976) Two-liquid partition coefficients: Experimental data and geochemical implications. Contributions to Mineralogy and Petrology, 56, 119–134.
——— (1977) Partitioning of manganese between forsterite and silicate liquid. Geochimica et Cosmochimica Acta, 41, 1363–1374.
Watson, E.B., and Harrison, T.M. (1983) Zircon saturation revisited: Temperature and composition effects in a variety of crustal magma types. Earth and Planetary Science Letters, 64, 295–304.
Wickham, S. (1987) Crustal anatexis and granite petrogenesis during low pressure regional metamorphism: The Trois Seigneurs Massif, Pyrenees, France. Journal of Petrology, 28, 127–169.
Wolf, M.B., and London, D. (1994) Apatite dissolution into peraluminous haplogranitic melts: An experimental study of solubilities and mechanisms. Geochimica et Cosmochimica Acta, 58, 4127–4145.
Wörner, G., Beusen, J.-M., Duchateau, N., Gijbels, R., and Schmincke, H.-U. (1983) Trace element abundances and mineral/melt distribution coefficients in phonolites from the Laacher See Volcano (Germany). Contributions to Mineralogy and Petrology, 84, 152–173.
Yoder, H.S., and Eugster, H.P. (1955) Synthetic and natural muscovites. Geochimica et Cosmochimica Acta, 8, 225–280.

Manuscript received July 2, 1995
Manuscript accepted January 26, 1996